Earth Syst. Dynam. Discuss., doi:10.5194/esd-2017-46, 2017
Manuscript under review for journal Earth Syst. Dynam.
Discussion started: 24 May 2017

Contrasting terrestrial carbon cycle responses to the two strongest El Niño events: 1997-98 and 2015-16 El Niños

Jun Wang[1,2], Ning Zeng[2,3], Meirong Wang[4], Fei Jiang[1], Hengmao Wang[1], and Ziqiang Jiang[1]

[1]International Institute for Earth System Science, Nanjing University, Nanjing, China

[2] State Key Laboratory of Numerical Modelling for Atmospheric Sciences and Geophysical Fluid Dynamics, Institute of Atmospheric Physics, Beijing, China

[3]Department of Atmospheric and Oceanic Science and Earth System Science Interdisciplinary Center, University of Maryland, College Park, Maryland, USA

[4]Collaborative Innovation Center on Forest and Evaluation of Meteorological Disasters/Key Laboratory of Meteorological Disaster of Ministry of Education, Nanjing University of Information Science & Technology, Nanjing, China

Correspondence to: J. Wang (wangjun@nju.edu.cn)

Abstract

The large interannual CO_2 variability is dominated by the response of terrestrial biosphere to El Niño-Southern Oscillation (ENSO). However, behaviors of terrestrial ecosystems differ in patterns and biological processes in different El Niño events. Here we conduct a comprehensive comparison of the two strongest El Niño events in history, namely, the recent 2015-16 event, and the earlier 1997-98 event in the context of multi-event 'composite' El Niño. We analyze Mauna Loa CO_2 concentration, surface carbon fluxes from three atmospheric inversions, and a mechanistic carbon cycle model VEGAS. We find large differences in the carbon cycle responses, even though the two El Nino events are of similar magnitude.

We find that the land-atmosphere carbon flux (F_{TA}) anomaly in 1997-98 El Niño was

Earth Syst. Dynam. Discuss., doi:10.5194/esd-2017-46, 2017
Manuscript under review for journal Earth Syst. Dynam.
Discussion started: 24 May 2017

Earth System Dynamics Discussions

1.95 Pg C yr^{-1} globally, but two times smaller during 2015-16 El Niño at 0.79 Pg C yr^{-1}. We also find that F_{TA} had no obvious lagged response in 2015-16 El Niño, in contrast to that in 1997-98 El Niño. Separating the global flux by major geographical regions, during 1997-98, the fluxes in the tropics and extratropical northern hemisphere were 1.98 and −0.04 Pg C yr^{-1}, respectively. During 2015-16, these were 1.07 and −0.4 Pg C yr^{-1}. Analysis of the mechanism shows that in the tropics, the widespread drier and warmer conditions caused the decrease in gross primary productivity (GPP, −1.11 Pg C yr^{-1}) and increase in terrestrial ecosystem respiration (TER, 0.49 Pg C yr^{-1}) in 1997-98 El Niño. During 2015-16, in contrast, anomalously wet conditions occurred in Sahel and East Africa that caused increase in GPP, compensating its decrease over other tropical regions. As a result, the total 2015-16 tropical GPP and TER anomalies were 0.29 and 1.23 Pg C yr^{-1}. GPP dominance during 1997-98 and TER dominance during 2015-16 accounted for the phase difference in their F_{TA}. In extratropical northern hemisphere, we find that temperature was warmer both in 1997-98 and 2015-16 El Niños over North America, contributing to enhancements in GPP and TER. However, temperature over Eurasia was warmer in 2015-16 El Niño, opposing to the cooler in 1997-98 and composite El Niño events. This warmer condition enhanced GPP and TER over the Eurasia in 2015-16 El Niño, compared to their suppressions in 1997-98 El Niño. The total extratropical northern hemisphere GPP and TER anomalies were 0.86 and 0.74 Pg C yr^{-1} in 1997-98 El Niño and 1.8 and 1.47 Pg C yr^{-1} in 2015-16 El Niño. Additionally, we find that wildfires played less important roles in 2015-16 El Niño than in 1997-98 El Niño.

Earth Syst. Dynam. Discuss., doi:10.5194/esd-2017-46, 2017
Manuscript under review for journal Earth Syst. Dynam.
Discussion started: 24 May 2017

Earth System Dynamics
Discussions
Open Access

1 Introduction

The atmospheric CO_2 growth rate has a significant interannual variability, greatly influenced by the El Niño-Southern Oscillation (ENSO) (Bacastow, 1976; Keeling et al., 1995). This interannual variability primarily stems from terrestrial ecosystems (Bousquet et al., 2000; Zeng et al., 2005). Further, there is a general consensus that the tropical terrestrial ecosystems account for the terrestrial carbon variability (Cox et al., 2013; Peylin et al., 2013; Wang et al., 2016; Wang et al., 2013; Zeng et al., 2005). They tend to anomalously release C flux during El Niño episodes, and uptake during La Nina episodes (Wang et al., 2016; Zeng et al., 2005). Recently, Ahlstrom et al. (2015) further suggested that ecosystems over the semi-arid regions dominated the terrestrial carbon interannual variability with its 39% contribution.

The terrestrial dominance primarily results from the drive-response mechanisms in climate variability (especially in temperature and precipitation) caused by ENSO and plants/soil physiology (Jung et al., 2017; Tian et al., 1998; Wang et al., 2016; Zeng et al., 2005). Directly, land-atmosphere C flux (F_{TA}) is mainly attributable to the imbalance between the gross primary productivity (GPP) and terrestrial ecosystem respiration (TER), according to $F_{TA} = TER - GPP + C_{fire}$ (C_{fire} is generally much smaller than GPP or TER). So variations in each of them or both result in the variations in F_{TA}.

Based on a dynamical global vegetation model (DGVM), Zeng et al. (2005) pointed out that net primary productivity (NPP) contributed to almost three fourth of the tropical F_{TA} interannual variability. Later, multi-model simulations involved in TRENDY project consistently suggested NPP or GPP dominated the terrestrial carbon variability (Ahlstrom et al., 2015; Piao et al., 2013; Wang et al., 2016).

These biological process analyses inferred that precipitation variation was the dominant climate factor in controlling F_{TA} interannual variability (Ahlstrom et al., 2015; Qian et al., 2008; Tian et al., 1998; Wang et al., 2016; Zeng et al., 2005). Quantitatively, Qian et al. (2008) illustrated the contributions of the tropical precipitation and temperature were 56 and 44% respectively, based on the model sensitivity experiments. Eddy covariance network observations suggested that interannual C flux variability over the tropical and temperate regions was controlled by precipitation, while boreal ecosystem C fluxes were more subject to temperature and radiation (Jung et al., 2011). At the same time, there was a significant positive correlation between atmospheric CO_2 growth rate and mean tropical land temperature (Anderegg et al., 2015; Cox et al., 2013; Wang et al., 2013; Wang et al., 2014). Sensitivity analysis indicated an about 3.5 Pg C yr^{-1} anomaly in CO_2 growth rate with a 1℃ increase in tropical land temperature, whereas only a weaker interannual coupling existed between CO_2 growth rate and tropical land precipitation (Wang et al., 2013). Therefore, these studies (Anderegg et al., 2015; Cox et al., 2013; Wang et al., 2013; Wang et al., 2014) suggested the temperature dominance in F_{TA} or CO_2 growth rate interannual variations, considering this strong emergent linear relationship. Recently, in order to reconcile these contradictory reports, Jung et al. (2017) illustrated that temporal and spatial compensatory effects in water availability linked yearly global F_{TA} variability to temperature.

Apart from these long-term time series studies on the interannual F_{TA} or CO_2 growth rate variability, we should keep in mind that the response of terrestrial carbon cycle to every El Niño/La Nina event has its unique behaviors such as in the strength, spatial pattern, biological process, and so on (Schwalm, 2011). For example, the wildfires played an important role in F_{TA} anomalies during 1997-98 El Niño (van der Werf et al., 2004). Recently, one of the three strongest El Niño events in recorded history occurred in 2015-16 years (https://www.esrl.noaa.gov/psd/enso/current.html). Given the

Earth Syst. Dynam. Discuss., doi:10.5194/esd-2017-46, 2017
Manuscript under review for journal Earth Syst. Dynam.
Discussion started: 24 May 2017

disturbance of the El Chichón eruption in 1982-83 El Niño episode, we here attempt to comprehensively compare the responses of terrestrial ecosystems to the two strongest El Niños in 1997-98 and 2015-16 years in the context of multi-event 'composite' El Nino, based on DGVM VEGAS in its Near-Real Time framework, inversion datasets (CAMS, MACC, and CarbonTracker) and so on. Our purpose is to clarify the distinctions in responses of biological processes in these two extreme events.

This paper is organized as follows: Section 2 describes the mechanistic carbon cycle model used, its drivers, and reference datasets. Section 3 presents the results about the total terrestrial C flux anomalies and spatial patterns along with their mechanisms. Finally, discussions and concluding remarks are illustrated in Sect. 4.

2 Model and datasets

2.1 Mechanistic carbon cycle model and its drivers

In this study, we used the state-of-the-art VEGAS version 2.4 in its Near-Real Time framework to investigate the responses of terrestrial ecosystems to El Niño events. VEGAS has been widely used to study the terrestrial carbon cycle on its seasonal cycle, interannual variability, and long-term trend (Zeng et al., 2005; Zeng et al., 2004; Zeng et al., 2014). And it extensively participated in the international carbon modelling project, such as the Coupled Climate-Carbon Cycle Model Intercomparison Project (C^4MIP) (Friedlingstein et al., 2006), TRENDY project (Sitch et al., 2015) and Multi-scale Synthesis and Terrestrial Model Intercomparison Project (MsTMIP) (Huntzinger et al., 2013). The detailed descriptions on its model structure, biological processes, and so on can be referred to the appendix in Zeng et al. (2005). We ran VEGAS on the 0.5°×0.5° horizontal resolution from 1901 till the end of year 2016, and focus on the period from 1980 to 2016.

Earth Syst. Dynam. Discuss., doi:10.5194/esd-2017-46, 2017
Manuscript under review for journal Earth Syst. Dynam.
Discussion started: 24 May 2017

The climate fields used to force VEGAS are as follows: (1) Precipitation datasets are generated by combining the Climatic Research Unit (CRU) Time-series (TS) Version 3.22 (University of East Anglia Climatic Research Unit et al., 2014) , NOAA's PRECipitation REConstruction over Land (PREC/L) (Chen et al., 2002), and NOAA NCEP climate anomaly monitoring system-outgoing longwave radiation precipitation index (CAMS-OPI) (Janowiak and Xie, 1999). (2) Temperature is adopted from the CRU TS3.22 before the year 2013, and generated by combining CRU 1981-2010 climatology and the Goddard Institute for Space Studies (GISS) Surface Temperature Analysis (GISTEMP) (Hansen et al., 2010) after 2013. (3) Downward shortwave radiation is retrieved from the driver datasets in MsTMIP (Wei et al., 2014) before the year 2010, and repeated the value of the year 2010 after it. Additionally, the gridded cropland and pasture land use datasets are integrated from the History Database of the Global Environment (HYDE) (Klein Goldewijk et al., 2011) with an linear extrapolation in 2016.

2.2 Reference datasets

We here take a series of reference datasets as a comparison with the simulation of VEGAS. The atmospheric CO_2 concentrations are from the monthly in-situ CO_2 datasets at Mauna Loa Observatory, Hawaii (Keeling et al., 1976). The Niño 3.4 (120°W–170°W, 5°S–5°N) sea surface temperature anomalies (SSTA) are adopted from the NOAA Extended Reconstructed Sea Surface Temperature (ERSST), version 4 (Huang et al., 2015), with a 3-month running average. We take Copernicus Atmosphere Monitoring Service (CAMS, 1980–2015), Monitoring atmospheric composition & climate (MACC, 1980–2014) inversion results (Chevallier, 2013), and CarbonTracker2016 (200001–201512) with the CarbonTracker Near-Real Time results in 2016 (Peters et al., 2007) to compare with VEGAS. Fire emissions come from the Global Fire Emissions Database, Version 4 (GFEDv4) from 1997 through 2014 (Randerson et al., 2015). Owing to the high correlation between solar-induced chlorophyll fluorescence (SIF) and terrestrial GPP (Guanter et al., 2014), we take the monthly satellite SIF from the GOME2_F version 26 from 2007 till 2016 (Joiner et al., 2012). Another, we adopt the Enhanced Vegetation Index (EVI) from MODIS MOD13C2 (Didan, 2015) to compare with the simulated leaf area index (LAI) anomalies.

In order to get the anomalies during the El Niño events, we first remove the long-term climatology in each dataset for getting rid of seasonal cycle signals, and then detrend them based on the linear regression, because the trend is not caused by the interannual variability.

3 Results

3.1 Total terrestrial C flux anomalies

Three strongest El Niño events (1982-83, 1997-98, and 2015-16) occurred from 1980 to 2016 with their maximum SST anomalies above 2.0 (Fig. 1a). El Niño event tends to make the atmospheric CO_2 growth rate anomalously increase (Fig. 1b), so there are two significant anomalously increased CO_2 growth rate corresponding to 1997-98 and 2015-16 El Niño events. Though the maximum increase in 2015-16 is a little smaller than that in 1997-98. Owing to the diffuse light disturbance (Mercado et al., 2009) of the eruption of Mount. El Chichón during 1982-83 El Niño event on the canonical coupling between CO_2 growth rate anomalies and El Niño events, we mainly focus on 1997-98 and 2015-16 El Niño events in this study. The interannual variability of atmospheric CO_2 growth rate principally originates from the terrestrial ecosystems (Fig.

Earth Syst. Dynam. Discuss., doi:10.5194/esd-2017-46, 2017
Manuscript under review for journal Earth Syst. Dynam.
Discussion started: 24 May 2017

1c). The correlation coefficient between CO_2 growth rate anomalies and global F_{TA} simulated by VEGAS is 0.64 ($p < 0.05$). In order to evaluate the performance of VEGAS simulation on the interannual time scale, we at the same time present CAMS, MACC and CarbonTracker inversion results. We find that CAMS and MACC inversions are nearly the same, both having the correlation coefficient about 0.60 ($p < 0.05$) with VEGAS. From 2000 through 2016, CarbonTracker is highly correlated with VEGAS ($r = 0.71$, $p < 0.05$). These high correlation coefficients between VEGAS and reference datasets underscore that VEGAS can well capture the terrestrial carbon cycle interannual variability.

There are altogether 10 El Niño events from 1980 through 2016, each with different duration and strength (Table 1). According to El Niño definition, we can find that these 10 El Niño events can be categorized into 2 weak (with a 0.5 to 0.9 SSTA), 3 moderate (1.0 to 1.4), 2 strong (1.5 to 1.9), and 3 very strong (≥2.0) events. In 1997-98 El Niño, the positive SSTA lasted from April 1997 to June 1998, while positive SSTA happened in winter 2014, and extended to June 2016 in 2015-16 El Niño (Fig. 2a). However, every El Niño event always peaks in winter (November or December) (Fig. 2a). Considering this phase-lock phenomenon in El Niño events, we make a composite analysis (getting rid of 1982-83 and 1991-92 because of the diffuse radiation disturbances) as the background responses of terrestrial carbon cycle to El Niño events. We can easily find that evolutions of F_{TA} anomalies in VEGAS, mean of CAMS and MACC, and CarbonTraker in composite, 1997-98, and 2015-16 El Niño events are closely consistent with Mauna Loa CGR anomalies (Fig. 2b, c, and d). Peaks of F_{TA} and Mauna Loa CGR anomalies in 1997-98 and 2015-16 El Niños are much stronger than those in composite analysis. Importantly, there were significant terrestrial lagged responses in composite and 1997-98 El Niño events, with the peak of F_{TA} anomaly in

March to April in El Niño decaying year (Fig. 2b and c), consistent with previous studies (Qian et al., 2008; Wang et al., 2016). But this lagged terrestrial response disappeared in Mauna Loa CGR, VEGAS and CarbonTracker in 2015-16 El Niño (Fig. 2d). Further, in June 2016, the F_{TA} anomaly of VEGAS and CarbonTracker significantly dropped (sign changed), but Mauna Loa CGR dropped a little (no sign changed) (Fig. 2d). Similar phenomenon also occurred earlier from April to July 2015. In addition, we can know that the anomalous C release caused by El Niño lasts about from July in the El Niño developing year to October in the El Niño decaying year (Fig. 2b, c, and d). For simplicity, we calculate the total anomalies in next context during this period for all El Niño events, taking the terrestrial lagged responses into account (Wang et al., 2016).

According to major geographical regions, we separate global F_{TA} anomaly into extratropical northern hemisphere (23°N–90°N), tropical regions (23°S–23°N), and extratropical southern hemisphere (60°S–23°S). Because F_{TA} anomaly over the extratropical southern hemisphere is generally smaller, we mainly present the evolutions of F_{TA} over the extratropical northern hemisphere and tropical regions in Fig. 3. Comparing the global and tropical F_{TA} anomalies, we find that F_{TA} anomalies in tropical regions dominate the global F_{TA} in these events (Fig. 3b, d and f), in accord with previous conclusions (Peylin et al., 2013; Zeng et al., 2005). Additionally, F_{TA} anomalies over the extratropical northern hemisphere are nearly neutral in VEGAS during composite and 1997-98 El Niño events (Fig. 3a and c). But we find that there were obvious anomalous uptakes from April to September in 2016 simulated by VEGAS (Fig. 3e), compensating the release over the tropics (Fig. 3f). These anomalous uptakes made the global negative F_{TA} anomalies from May to September in 2016 (Fig. 2d). Similar anomalous uptake happened over the extratropical northern hemisphere

Earth Syst. Dynam. Discuss., doi:10.5194/esd-2017-46, 2017
Manuscript under review for journal Earth Syst. Dynam.
Discussion started: 24 May 2017

Earth System Dynamics
Discussions
Open Access

earlier from April to July 2015. These anomalous uptakes in VEGAS are to some extent consistent with results in CarbonTracker, and well account for the global F_{TA} drops mentioned above in these periods. Comparing the behaviors between Mauna Loa CGR and F_{TA} anomalies, we can now clearly find that Mauna Loa CGR, coming from the tropical observatory, does not reflect the signals over the extratropical northern hemisphere in time (Fig. 2d and Fig. 3e).

Because F_{TA} mainly stems from the difference between TER and GPP, we present TER and GPP anomalies in Fig. 4 in order to well explain the F_{TA} anomalies. We find that anomalous negative GPP dominated the F_{TA} anomaly in tropics during composite and 1997-98 El Niño episodes with the significant lagged responses (peak at about May in El Niño decaying year) (Fig. 4b and d). Besides, obvious positive TER anomalies occurred from October 1997 to April 1998 (Fig. 4d), contributing to tropical C release in this period (Fig. 3d). In contrast, we find that anomalous positive TER dominated the F_{TA} anomaly in tropics during 2015-16 El Niño episode without obvious lags (Fig. 4f), accounting for the disappearance of terrestrial F_{TA} lagged response (Fig. 2d). In the extratropical northern hemisphere, increased GPP and TER from April to October in composite and 1998 were nearly identical (Fig. 4a and c), making neutral F_{TA} anomalies (Fig. 3a and c). But increased GPP was stronger than increased TER from April to July 2015 and from April to September 2016 (Fig. 4e), resulting in the anomalous uptake in F_{TA} (Fig. 2d and Fig. 3e).

Quantitatively, we calculated the total C flux anomalies from July in El Niño developing year till October in El Niño decaying year. The composite global F_{TA} anomaly during El Niño events in VEGAS is about 0.71 Pg C yr^{-1}, dominated by tropical ecosystems with 0.74 Pg C yr^{-1} (Table 2). These anomalies are comparable to the mean of CAMS and MACC inversion results with 0.92 ± 0.01 globally and

0.66 ± 0.03 Pg C yr^{-1} in tropics. In these two extreme cases, a very strong anomalous C release occurred in 1997-98 El Niño episode with a value of 1.93 Pg C yr^{-1}, close to 2.57 Pg C yr^{-1} in CAMS and MACC inversions, while only 0.79 Pg C yr^{-1} was released in 2015-16 El Niño episode, comparable to 0.82 Pg C yr^{-1} in CarbonTracker. But F_{TA} anomalies in tropical regions dominated the global F_{TA} anomalies in both cases with respective values of 1.98 and 1.07 Pg C yr^{-1} in VEGAS. Moreover, anomalous C uptake simulated by VEGAS over the extratropical northern hemisphere cancelled 0.40 Pg C yr^{-1} anomalous release in tropics in 2015-16 El Niño, while it was neutral (−0.04 Pg C yr^{-1}) in 1997-98 El Niño. And the F_{TA} anomaly was relatively smaller in the extratropical southern hemisphere.

In biological processes, GPP (−1.11 Pg C yr^{-1}) and TER (0.49 Pg C yr^{-1}) in tropics together drove the anomalous F_{TA} in 1997-98, while TER (1.23 Pg C yr^{-1}) partly cancelled by GPP (0.29 Pg C yr^{-1}) drove the anomalous F_{TA} in 2015-16 (Table 2). These data confirmed that GPP played the more important role in 1997-98, while TER dominance occurred in 2015-16 El Niño episode. In the extratropical northern hemisphere, GPP and TER cancelled each other. They had respective 0.20 and 0.12 Pg C yr^{-1} in composite analysis and 0.86 and 0.74 Pg C yr^{-1} in 1997-98 El Niño, making the nearly neutral F_{TA} anomaly there. But GPP (1.80 Pg C yr^{-1}) was stronger than TER (1.47 Pg C yr^{-1}) in 2015-16 El Niño, causing the significant C uptake. Additionally, F_{TA} anomaly caused by wildfires also played an important role in 1997-98 El Niño episode with globally 0.46 Pg C yr^{-1} in VEGAS, consistent with GFED fire data product (0.82 Pg C yr^{-1}). The effect of wildfires on F_{TA} anomaly in 1997-98 El Niño episode has been suggested by van der Werf et al. (2004). But it was close to zero (0.08 Pg C yr^{-1}) in 2015-16 El Niño episode.

Earth Syst. Dynam. Discuss., doi:10.5194/esd-2017-46, 2017
Manuscript under review for journal Earth Syst. Dynam.
Discussion started: 24 May 2017

Earth System Dynamics
Open Access
Discussions

3.2 Spatial features and its mechanisms

Regional responses of terrestrial ecosystems to El Niño events are inhomogeneous, principally according to the anomalies in climate variability. In composite El Niño analysis (Fig. 5a), land consistently releases C flux in tropics, while it anomalously uptakes C flux over North America as well as the central and eastern Europe. These regional responses are generally consistent with the CAMS and MACC inversion results (Fig. 5d).

In 1997-98 El Niño episode, tropical responses were analogous to composite results except the stronger releases. North America and central and eastern China had stronger C uptake, whereas Europe and Russia had stronger C release (Fig. 5b). However, in 2015-16 El Niño episode, anomalous C uptake happened over the Sahel and east Africa, compensating the C release over the other tropical regions (Fig. 5c). It made the total F_{TA} anomaly in tropics in 2015-16 smaller than that in 1997-98 (Fig. 3d and f, and Table 2). North America had anomalous C uptake, similar to that in composite and 1997-98 El Niño, while central and eastern Russia also had anomalous C uptake in 2015-16 El Niño (Fig. 5c), opposing to C release in composite and 1997-98 El Niño. This opposing behavior of boreal forests over the central and eastern Russia clearly contributed to the total uptake over the extratropical northern hemisphere (Table 2). Moreover, we can clearly find that these regional responses in 2015-16 El Niño episode are significantly consistent with the CarbonTracker result (Fig. 5f).

In order to better make the explanations on these regional C flux anomalies, we present the main climate variabilities of soil wetness (mainly caused precipitation) and air temperature, as well as the biological processes of GPP and TER in Fig. 6. In the composite analyses, the soil wetness is generally reduced in tropics (Fig. 6a), making the widespread decrease in GPP (Fig. 6b), verified by model sensitivity experiments

Earth Syst. Dynam. Discuss., doi:10.5194/esd-2017-46, 2017
Manuscript under review for journal Earth Syst. Dynam.
Discussion started: 24 May 2017

(Qian et al., 2008). At the same time, air temperature is anomalously warmer, contributing to the enhancement in TER. But the drier conditions in the semi-arid regions such as Sahel, South Africa, and Australia, restrict the enhancement in TER induced by warmer temperature (Fig. 6d). Higher air temperature over the North America largely enhances GPP and TER, while cooler conditions over the Eurasia will reduce them (Fig. 6b–d). Wetter conditions over part of North America and Eurasia also to some extent benefit GPP and TER (Fig. 6a).

Comparing the composite results (Fig. 6a–d) and 1997-98 El Niño episode (Fig.6e–h), we can easily find that the regional patterns are almost identical except the difference in magnitude. In contrast, there are some differences in 2015-16 El Niño episode. Over the Sahel and East Africa, the soil wetness increased induced by more precipitation (Fig. 6i), dynamically making the air temperature cooler (Fig. 6k). This wetter condition largely benefit GPP (Fig. 6j), compensating the decreased GPP over the other tropical regions. It caused in total the increased GPP in tropics, opposing to composite and 1997-98 El Niño episode (Table 2). More soil moisture also contributed to increase in TER over the Sahel (Fig. 6l), contrary to that in 1997-98 El Niño episode (Fig. 6h). This spatial compensation in GPP together with the widespread increased TER well accounted for the TER dominance in tropics during 2015-16 El Niño episode. Besides, increased GPP resulted in the anomalous C uptake here (Fig. 5c) which partly compensated the anomalous C release over the other tropical regions. It in some degree made the tropical smaller F_{TA} in 2015-16 El Niño episode than that in 1997-98 El Niño episode. Another obvious difference happened over the Eurasia with almost opposite signals in 1997-98 and 2015-16 El Niño episodes. Air temperature during 2015-16 El Niño episode over the Eurasia was anomalously higher, opposing to the cooler during composite and 1997-98 El Niño (Fig. 6c, g, and k). This warmer condition enhanced

Earth Syst. Dynam. Discuss., doi:10.5194/esd-2017-46, 2017
Manuscript under review for journal Earth Syst. Dynam.
Discussion started: 24 May 2017

GPP and TER (Fig. 6j and l), contrary to their suppressions in composite and 1997-98 El Niño (Fig. 6b, d, f, and h). This phenomenon explained stronger GPP and TER anomalies and anomalous C uptake over the whole extratropical northern hemisphere (Table 2).

Recently, more attentions have been paid on SIF as an effective indicator for GPP (Guanter et al., 2014). Therefore, we here try to make a comparison between simulated GPP and SIF variabilities on the interannual timescale. Though there are noisy signals in SIF, we can find that SIF was anomalously positive over the USA, part of Europe, and East Africa, and negative over the Amazon and South Asia during the 2015-16 El Niño episode, corresponding to the increased and decreased GPP respectively (Fig. 7a and c). The correspondences over the other regions were not significant. In addition, MODIS EVI anomalously increased over the America, Southern South America, part of Europe, Sahel, and East Africa, but decreases over the Amazon, Northern Canada, central Africa, South Asia, and Northern Australia (Fig. 7d). These EVI anomalies were well corresponding to simulated LAI anomalies (Fig. 7b). These good correspondences between simulated GPP (LAI) and SIF (EVI) give us more confidence in VEGAS simulations.

At last, wildfires as important disturbances for F_{TA} always release C flux. Though F_{TA} anomalies caused by wildfires are generally smaller than GPP or TER anomalies, they played an important role in 1997-98 El Niño episode (Globally 0.46 Pg C yr^{-1} in VEGAS and 0.82 Pg C yr^{-1} in GFED) (Table 2), consistent with the previous study (van der Werf et al., 2004). Here we show the F_{TA} anomalies caused by wildfires in Fig. 8. The correlation coefficients between simulated global F_{TA} anomalies caused by wildfires and GFED fire data product are 0.40 (unsmoothed) and 0.61 (smoothed) (Fig. 8a), confirming that VEGAS has certain capability in simulating this disturbance. In

1997-98 El Niño episode, satellite-based GFED data showed that F_{TA} anomalies caused by wildfires mainly happened over the tropical regions, such as Amazon, Central Africa, South Asia, and Indonesia (Fig. 8d). VEGAS also simulated the positive F_{TA} over these tropical regions (Fig. 8b). The total tropical F_{TA} anomalies caused by fires were 0.39 Pg C yr^{-1} in VEGAS and 0.72 Pg C yr^{-1} in GFED (Table 2). In 2015-16 El Niño episode, wildfires also resulted in positive F_{TA} anomalies over Amazon, South Asia, and Indonesia, but their magnitudes were smaller than those in 1997-98 El Niño episode, because it was much drier in 1997-98 El Niño episode than in 2015-16 El Niño episode (Fig. 6e and i). In addition, the wetter conditions over the East Africa in 2015-16 El Niño episode depressed the occurrences of wildfires with the negative F_{TA} anomalies (Fig. 8c). The tropical F_{TA} anomaly in total was 0.13 Pg C yr^{-1} in VEGAS (Table 2). Therefore, we can find that wildfires played less important roles in 2015-16 than in 1997-98 El Niño episode. F_{TA} anomalies caused by wildfires over the extratropics are much weaker than those over the tropics, and their correspondences between VEGAS and GFED are poorer (Table 2 and Fig. 8b and d).

4 Conclusions and Discussions

Climate anomalies in magnitudes and patterns caused by different El Niño events are inconsistent, so responses of terrestrial ecosystems remain uncertain to different El Niño events (Schwalm, 2011). In this study, we comprehensively compare the impacts of the two strongest El Niño events in history, namely, the recent 2015-16, and earlier 1997-98 events in the context of multi-event 'composite' El Nino on the terrestrial carbon cycle, relying on VEGAS in its Near-Real Time framework, inversion datasets and so on. Main conclusions are drawn as follows:

(1) Simulations indicate that F_{TA} anomaly in 2015-16 El Niño episode was globally

Earth Syst. Dynam. Discuss., doi:10.5194/esd-2017-46, 2017
Manuscript under review for journal Earth Syst. Dynam.
Discussion started: 24 May 2017

0.79 Pg C yr^{-1}, nearly two times smaller than that in 1997-98 El Niño (1.95 Pg C yr^{-1}), confirmed by inversion results. We also find that F_{TA} had no obvious lagged response in 2015-16 El Niño, in contrast to that in 1997-98 El Niño. Separating the global flux, we find that fluxes in the tropics and extratropical northern hemisphere were 1.07 and −0.4 Pg C yr^{-1} during 2015-16 El Niño episode respectively, while these were 1.98 and −0.04 Pg C yr^{-1} during 1997-98 event. Tropical F_{TA} anomalies dominated global F_{TA} anomalies in both extreme El Niño events.

(2) Mechanistic analysis indicates that anomalously wetter conditions happened over the Sahel and East Africa during 2015-16 El Niño episode, resulting in the increase of GPP, which compensated the reduction of GPP over the other tropical regions. It caused in total the increased GPP in tropics (0.29 Pg C yr^{-1}), opposing to composite analysis (−0.80 Pg C yr^{-1}) and 1997-98 El Niño (−1.11 Pg C yr^{-1}). Spatial compensation in GPP and widespread increased TER (1.23 Pg C yr^{-1}) well explained the TER dominance in 2015-16 El Niño episode, opposing to GPP dominance in 1997-98 event. Different biological dominance accounted for the phase difference in F_{TA} responses in 1997-98 and 2015-16 El Niños.

(3) Higher air temperature over the North America largely enhanced GPP and TER both in 1997-98 and 2015-16 El Niño episodes. However, air temperature during 2015-16 El Niño episode over the Eurasia was anomalously higher, opposing the cooler in 1997-98 El Niño episode. This warmer condition benefited GPP and TER, well accounting for stronger GPP (1.80 Pg C yr^{-1}) and TER (1.47 Pg C yr^{-1}) anomalies and anomalous C uptake (−0.40 Pg C yr^{-1}) over the extratropical northern hemisphere during 2015-16 El Niño.

(4) Wildfires, frequently happening in tropics, played an important role in F_{TA} anomalies during 1997-98 El Niño episode, confirmed by VEGAS simulation and

satellite-based GFED fire product. But VEGAS simulation indicates that the tropical F_{TA} caused by wildfires during 2015-16 El Niño episode was relatively smaller than that during 1997-98 El Niño episode. This result was mainly because the tropical weather was much drier in 1997-98 El Niño than that in 2015-16 El Niño.

Data Availability

In this study, all the datasets can be freely accessed. Mauna Loa monthly CO_2 records are available at https://www.esrl.noaa.gov/gmd/ccgg/trends/data.html. ERSST4 Niño3.4 index can be accessed from http://www.cpc.ncep.noaa.gov/data/indices/ersst4.nino.mth.81-10.ascii. CAMS and MACC inversions are available at http://apps.ecmwf.int/datasets/. CarbonTracker datasets can be found at https://www.esrl.noaa.gov/gmd/ccgg/carbontracker/. GFEDv4 global fire emissions are downloaded at https://daac.ornl.gov/cgi-bin/dsviewer.pl?ds_id=1293. Satellite SIF datasets are retrieved from http://avdc.gsfc.nasa.gov/pub/data/satellite/MetOp/GOME_F/MetOp-A/level3/. MODIS enhanced vegetation index (EVI) datasets are downloaded from https://lpdaac.usgs.gov/dataset_discovery/modis/modis_products_table/mod13c2_v006.

Acknowledgements:

We gratefully appreciate the ESRL for the use of their Mauna Loa atmospheric CO_2 records and CarbonTracker datasets, NOAA for ERSST4 ENSO index, LSCE-IPSL for CAMS and MACC inversion datasets, the Oak Ridge National Laboratory Distributed Active Archive Center for GFEDv4 global fire emissions, NASA Goddard Space Flight

Center for SIF datasets, and Land Processes Distributed Active Archive Center for MODIS EVI datasets.

References

Ahlstrom, A., Raupach, M. R., Schurgers, G., Smith, B., Arneth, A., Jung, M., Reichstein, M., Canadell, J. G., Friedlingstein, P., Jain, A. K., Kato, E., Poulter, B., Sitch, S., Stocker, B. D., Viovy, N., Wang, Y. P., Wiltshire, A., Zaehle, S., and Zeng, N.: The dominant role of semi-arid ecosystems in the trend and variability of the land CO_2 sink, Science, 348, 895-899, 2015.

Anderegg, W. R., Ballantyne, A. P., Smith, W. K., Majkut, J., Rabin, S., Beaulieu, C., Birdsey, R., Dunne, J. P., Houghton, R. A., Myneni, R. B., Pan, Y., Sarmiento, J. L., Serota, N., Shevliakova, E., Tans, P., and Pacala, S. W.: Tropical nighttime warming as a dominant driver of variability in the terrestrial carbon sink, Proc Natl Acad Sci U S A, 112, 15591-15596, 2015.

Bacastow, R. B.: Modulation of atmospheric carbon dioxide by the Southern Oscillation, Nature, 261, 116-118, 1976.

Bousquet, P., Peylin, P., Ciais, P., Le Quere, C., Friedlingstein, P., and Tans, P. P.: Regional changes in carbon dioxide fluxes of land and oceans since 1980, Science, 290, 1342-1346, 2000.

Chen, M., Xie, P., Janowiak, J. E., and Arkin, P. A.: Global Land Precipitation: A 50-yr Monthly Analysis Based on Gauge Observations, Journal of Hydrometeorology, 3, 249-266, 2002.

Chevallier, F.: On the parallelization of atmospheric inversions of CO_2 surface fluxes within a variational framework, Geosci Model Dev, 6, 783-790, 2013.

Cox, P. M., Pearson, D., Booth, B. B., Friedlingstein, P., Huntingford, C., Jones, C. D., and Luke, C. M.: Sensitivity of tropical carbon to climate change constrained by carbon dioxide variability, Nature, 494, 341-344, 2013.

Didan, K.: MOD13C2 MODIS/Terra Vegetation Indices Monthly L3 Global 0.05Deg CMG V006. NASA EOSDIS Land Processes DAAC. https://doi.org/10.5067/MODIS/MOD13C2.006, 2015

Friedlingstein, P., Cox, P., Betts, R., Bopp, L., Von Bloh, W., Brovkin, V., Cadule, P., Doney, S., Eby, M., Fung, I., Bala, G., John, J., Jones, C., Joos, F., Kato, T., Kawamiya, M., Knorr, W., Lindsay, K., Matthews, H. D., Raddatz, T., Rayner, P., Reick, C., Roeckner, E., Schnitzler, K. G., Schnur, R., Strassmann, K., Weaver, A. J., Yoshikawa, C., and Zeng, N.: Climate-carbon cycle feedback analysis: Results from the C^4MIP model intercomparison, Journal of Climate, 19, 3337-3353, 2006.

Guanter, L., Zhang, Y. G., Jung, M., Joiner, J., Voigt, M., Berry, J. A., Frankenberg, C., Huete, A. R., Zarco-Tejada, P., Lee, J. E., Moran, M. S., Ponce-Campos, G., Beer, C., Camps-Valls, G., Buchmann, N., Gianelle, D., Klumpp, K., Cescatti, A., Baker, J. M., and Griffis, T. J.: Global and time-resolved monitoring of crop photosynthesis with chlorophyll fluorescence, PNAS, doi: 0.1073/pnas.1320008111, 2014. E1327–E1333, 2014.

Hansen, J., Ruedy, R., Sato, M., and Lo, K.: Global Surface Temperature Change, Reviews of Geophysics, 48, 2010.

Huang, B., Banzon, V. F., Freeman, E., Lawrimore, J., Liu, W., Peterson, T. C., Smith, T. M., Thorne, P. W., Woodruff, S. D., and Zhang, H.-M.: Extended Reconstructed Sea Surface Temperature Version 4 (ERSST.v4). Part I: Upgrades and Intercomparisons, Journal of Climate, 28, 911-930, 2015.

Huntzinger, D. N., Schwalm, C., Michalak, A. M., Schaefer, K., King, A. W., Wei, Y., Jacobson, A., Liu, S., Cook, R. B., Post, W. M., Berthier, G., Hayes, D., Huang, M., Ito, A., Lei, H., Lu, C., Mao, J., Peng, C. H., Peng, S., Poulter, B., Riccuito, D., Shi, X., Tian, H., Wang, W., Zeng, N., Zhao, F., and Zhu, Q.: The North American Carbon Program Multi-Scale Synthesis and Terrestrial Model Intercomparison Project – Part 1: Overview and experimental design, Geosci Model Dev, 6, 2121-2133, 2013.

Janowiak, J. E. and Xie, P.: CAMS-OPI: A Global Satellite-Rain Gauge Merged Product for Real-Time Precipitation Monitoring Applications, J. Clim., 12, 3335-3342, 1999.

Joiner, J., Yoshida, Y., Vasilkov, A. P., Middleton, E. M., Campbell, P. K. E., Yoshida, Y., Kuze, A., and Corp, L. A.: Filling-in of near-infrared solar lines by terrestrial fluorescence and other geophysical effects: simulations and space-based observations from SCIAMACHY and GOSAT, Atmospheric Measurement Techniques, 5, 809-829, 2012.

Jung, M., Reichstein, M., Margolis, H. A., Cescatti, A., Richardson, A. D., Arain, M. A., Arneth, A., Bernhofer, C., Bonal, D., Chen, J. Q., Gianelle, D., Gobron, N., Kiely, G., Kutsch, W., Lasslop, G., Law, B. E., Lindroth, A., Merbold, L., Montagnani, L., Moors, E. J., Papale, D., Sottocornola, M., Vaccari, F., and Williams, C.: Global patterns of land-atmosphere fluxes of carbon dioxide, latent heat, and sensible heat derived from eddy covariance, satellite, and meteorological observations, J Geophys Res-Biogeo, 116, 2011.

Jung, M., Reichstein, M., Schwalm, C. R., Huntingford, C., Sitch, S., Ahlstrom, A., Arneth, A., Camps-Valls, G., Ciais, P., Friedlingstein, P., Gans, F., Ichii, K., Jain, A. K., Kato, E., Papale, D., Poulter, B., Raduly, B., Rodenbeck, C., Tramontana, G., Viovy, N., Wang, Y. P., Weber, U., Zaehle, S., and Zeng, N.: Compensatory water effects link yearly global land CO_2 sink changes to temperature, Nature, 541, 516-520, 2017.

Keeling, C. D., Bacastow, R. B., Bainbridge, A. E., Ekdahl, C. A., Guenther, P. R.,

Earth Syst. Dynam. Discuss., doi:10.5194/esd-2017-46, 2017
Manuscript under review for journal Earth Syst. Dynam.
Discussion started: 24 May 2017

Earth System Dynamics
Open Access
Discussions

Waterman, L. S., and Chin, J. F. S.: Atmospheric Carbon-Dioxide Variations at Mauna-Loa Observatory, Hawaii, Tellus, 28, 538-551, 1976.

Keeling, C. D., Whorf, T. P., Wahlen, M., and Vanderplicht, J.: Interannual Extremes in the Rate of Rise of Atmospheric Carbon-Dioxide since 1980, Nature, 375, 666-670, 1995.

Klein Goldewijk, K., Beusen, A., Van Drecht, G., and De Vos, M.: The HYDE 3.1 spatially explicit database of human-induced global land-use change over the past 12,000 years, Global Ecology and Biogeography, 20, 73-86, 2011.

Mercado, L. M., Bellouin, N., Sitch, S., Boucher, O., Huntingford, C., Wild, M., and Cox, P. M.: Impact of changes in diffuse radiation on the global land carbon sink, Nature, 458, 1014-U1087, 2009.

Peters, W., Jacobson, A. R., Sweeney, C., Andrews, A. E., Conway, T. J., Masarie, K., Miller, J. B., Bruhwiler, L. M., Petron, G., Hirsch, A. I., Worthy, D. E., van der Werf, G. R., Randerson, J. T., Wennberg, P. O., Krol, M. C., and Tans, P. P.: An atmospheric perspective on North American carbon dioxide exchange: CarbonTracker, Proc Natl Acad Sci U S A, 104, 18925-18930, 2007.

Peylin, P., Law, R. M., Gurney, K. R., Chevallier, F., Jacobson, A. R., Maki, T., Niwa, Y., Patra, P. K., Peters, W., Rayner, P. J., Rödenbeck, C., van der Laan-Luijkx, I. T., and Zhang, X.: Global atmospheric carbon budget: results from an ensemble of atmospheric CO_2 inversions, Biogeosciences, 10, 6699-6720, 2013.

Piao, S., Sitch, S., Ciais, P., Friedlingstein, P., Peylin, P., Wang, X., Ahlström, A., Anav, A., Canadell, J. G., Cong, N., Huntingford, C., Jung, M., Levis, S., Levy, P. E., Li, J., Lin, X., Lomas, M. R., Lu, M., Luo, Y., Ma, Y., Myneni, R. B., Poulter, B., Sun, Z., Wang, T., Viovy, N., Zaehle, S., and Zeng, N.: Evaluation of terrestrial carbon cycle models for their response to climate variability and to CO_2 trends, Global Change

Earth Syst. Dynam. Discuss., doi:10.5194/esd-2017-46, 2017
Manuscript under review for journal Earth Syst. Dynam.
Discussion started: 24 May 2017

Biology, doi: 10.1111/gcb.12187, 2013. 2117–2132, 2013.

Qian, H., Joseph, R., and Zeng, N.: Response of the terrestrial carbon cycle to the El Nino-Southern Oscillation, Tellus Series B-Chemical and Physical Meteorology, 60, 537-550, 2008.

Schwalm, C. R.: Does terrestrial drought explain global CO_2 flux anomalies induced by El Nino?, Biogeosciences, 8, 2493-2506, 2011.

Sitch, S., Friedlingstein, P., Gruber, N., Jones, S. D., Murray-Tortarolo, G., Ahlström, A., Doney, S. C., Graven, H., Heinze, C., Huntingford, C., Levis, S., Levy, P. E., Lomas, M., Poulter, B., Viovy, N., Zaehle, S., Zeng, N., Arneth, A., Bonan, G., Bopp, L., Canadell, J. G., Chevallier, F., Ciais, P., Ellis, R., Gloor, M., Peylin, P., Piao, S. L., Le Quéré, C., Smith, B., Zhu, Z., and Myneni, R.: Recent trends and drivers of regional sources and sinks of carbon dioxide, Biogeosciences, 12, 653-679, 2015.

Randerson, J. T., van der Werf, G. R., Giglio, L., Collatz, G. J. and Kasibhatla, P. S.:Global Fire Emissions Database, Version 4, (GFEDv4). ORNL DAAC, Oak Ridge, Tennessee, USA. http://dx.doi.org/10.3334/ORNLDAAC/1293, 2015.

Tian, H. Q., Melillo, J. M., Kicklighter, D. W., McGuire, A. D., Helfrich, J. V. K., Moore, B., and Vorosmarty, C. J.: Effect of interannual climate variability on carbon storage in Amazonian ecosystems, Nature, 396, 664-667, 1998.

University of East Anglia Climatic Research Unit, Harris, I.C., Jones, P.D.: CRU TS3.22: Climatic Research Unit (CRU) Time-Series (TS) Version 3.22 of High Resolution Gridded Data of Month-by-month Variation in Climate (Jan. 1901- Dec. 2013). NCAS British Atmospheric Data Centre, 2014.

van der Werf, G. R., Randerson, J. T., Collatz, G. J., Giglio, L., Kasibhatla, P. S., Arellano, A. F., Jr., Olsen, S. C., and Kasischke, E. S.: Continental-scale partitioning of fire emissions during the 1997 to 2001 El Nino/La Nina period, Science, 303, 73-76, 2004.

Wang, J., Zeng, N., and Wang, M.: Interannual variability of the atmospheric CO_2 growth rate: roles of precipitation and temperature, Biogeosciences, 13, 2339-2352, 2016.

Wang, W., Ciais, P., Nemani, R., Canadell, J. G., Piao, S., Sitch, S., White, M. A., Hashimoto, H., Milesi, C., and Myneni, R. B.: Variations in atmospheric CO_2 growth rates coupled with tropical temperature, PNAS, 110, 13061-13066, 2013.

Wang, X., Piao, S., Ciais, P., Friedlingstein, P., Myneni, R. B., Cox, P., Heimann, M., Miller, J., Peng, S., Wang, T., Yang, H., and Chen, A.: A two-fold increase of carbon cycle sensitivity to tropical temperature variations, Nature, 506, 212-215, 2014.

Wei, Y., Liu, S., Huntzinger, D. N., Michalak, A. M., Viovy, N., Post, W. M., Schwalm, C. R., Schaefer, K., Jacobson, A. R., Lu, C., Tian, H., Ricciuto, D. M., Cook, R. B., Mao, J., and Shi, X.: The North American Carbon Program Multi-scale Synthesis and Terrestrial Model Intercomparison Project – Part 2: Environmental driver data, Geosci Model Dev, 7, 2875-2893, 2014.

Zeng, N., Mariotti, A., and Wetzel, P.: Terrestrial mechanisms of interannual CO_2 variability, Global Biogeochemical Cycles, 19, GB1016, 2005.

Zeng, N., Qian, H. F., Munoz, E., and Iacono, R.: How strong is carbon cycle-climate feedback under global warming?, Geophys Res Lett, 31, 2004.

Zeng, N., Zhao, F., Collatz, G. J., Kalnay, E., Salawitch, R. J., West, T. O., and Guanter, L.: Agricultural Green Revolution as a driver of increasing atmospheric CO_2 seasonal amplitude, Nature, 515, 394-397, 2014.

Tables and Figures:

Table 1 Lists of El Niño events from 1980 till 2016.

No.	El Niño Events	Duration (mo)	Maximum Nino3.4 Index (℃)
1	Apr1982–Jun1983	15	2.1
2	Sep1986–Feb1988	18	1.6
3	Jun1991–Jul1992	14	1.6
4	Oct1994–Mar1995	6	1.0
5	May1997–May1998	13	2.3
6	Jun2002–Feb2003	9	1.2
7	Jul2004–Apr2005	10	0.7
8	Sep2006–Jan2007	5	0.9
9	Jul2009–Apr2010	10	1.3
10	Nov2014–May2016	19	2.3

Table 2 Carbon flux anomalies during El Niño events, calculated as the mean from July in the El Niño developing year to October in El Niño decaying year. Flux units are in Pg C yr^{-1}.

Zones	El Niños	Inversions		VEGAS Model				GFED
		F_{TA} (CAMS+MACC)[a]	F_{TA} (CarbonTracker)	F_{TA}	GPP	TER	C_{fire}	C_{fire}
Global	composite[b]	0.92±0.01	–	0.71	−0.76	−0.20	0.15	–
	1997-98	2.57±0.04	–	1.93	−0.11	1.36	0.46	0.82
	2015-16	–	0.82	0.79	1.79	2.50	0.08	–
NH	composite	0.20±0.02	–	−0.09	0.20	0.12	−0.01	–
	1997-98	0.40±0.07	–	−0.04	0.86	0.74	0.07	0.11
	2015-16	–	0.18	−0.40	1.80	1.47	−0.06	–
Tropical	composite	0.66±0.03	–	0.74	−0.80	−0.22	0.16	–

Earth Syst. Dynam. Discuss., doi:10.5194/esd-2017-46, 2017
Manuscript under review for journal Earth Syst. Dynam.
Discussion started: 24 May 2017

Earth System Dynamics
Discussions

	1997-98	2.12±0.14	–	1.98	−1.11	0.49	0.39	0.72
	2015-16	–	0.53	1.07	0.29	1.23	0.13	–
	composite	0.07±0.01	–	0.06	−0.16	−0.10	0.00	–
SH	1997-98	0.05±0.02	–	−0.01	0.13	0.13	0.00	−0.01
	2015-16	–	0.11	0.12	−0.31	−0.19	0.00	–

[a]It represents the mean value of CAMS and MACC inversion results with the uncertainty of their standard deviation.

[b]Composite analyses exclude 1982-83, 1991-92, and 2015-16 El Niños, because the former two cases are disturbed by eruptions of El Chichón and Pinatubo, and the latter is not covered by inversion datasets.

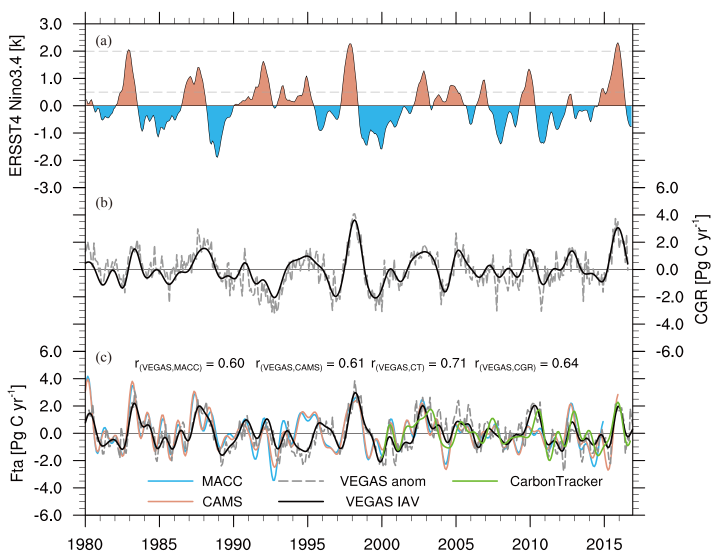

Figure 1. Interannual variabilities (IAV) in sea surface temperature anomaly (SSTA) and carbon cycle. (a) ERSST4 Niño3.4 Index (units: K). It is the 3-month running averaged SST anomaly for the Niño 3.4 region (5°N–5°S, 120°–170°W). (b) IAV in MLO CO_2 growth rate (CGR, units: Pg C yr^{-1}). CGR is calculated as the difference

Earth Syst. Dynam. Discuss., doi:10.5194/esd-2017-46, 2017
Manuscript under review for journal Earth Syst. Dynam.
Discussion started: 24 May 2017

Earth System Dynamics
Discussions
Open Access

between the monthly mean in the adjacent years. The dashed line is the detrended anomaly and the solid line is smoothed by the butterworth filtering. (c) IAV in land-atmosphere carbon fluxes (F_{TA}, units: Pg C yr^{-1}). Blue and orange solid lines are the smoothed results of MACC and CAMS inversions. Gray dashed line is the detrended anomaly and black one is the smoothed result in VEGAS model simulation. The green solid line is the smoothed CarbonTracker result.

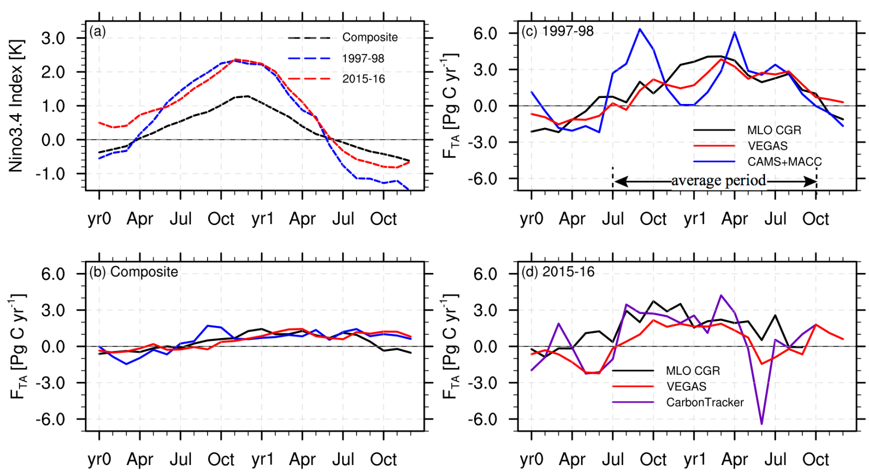

Figure 2. Evolutions of global F_{TA} along with the development of El Niño. (a) shows the SSTA in composite (in black), 1997-98 (in blue), and 2015-16 (in red) El Niño events. (b) illustrate the F_{TA} anomalies in El Niño composite analysis. The black solid line denotes Mauna Loa CGR; red and blue lines show the VEGAS and mean of CAMS and MACC inversions, respectively. (c) shows the F_{TA} anomalies during 1997-98 El Niño events. And the arrows demonstrate the time periods during which we calculate the C flux anomalies in table and below space figures. (d) demonstrate the F_{TA} anomalies during 2015-16 El Niño events. And the purple line denotes result of CarbonTracker2016 and CarbonTracker Near Real-Time datasets.

Earth Syst. Dynam. Discuss., doi:10.5194/esd-2017-46, 2017
Manuscript under review for journal Earth Syst. Dynam.
Discussion started: 24 May 2017

Earth System Dynamics
Open Access
Discussions

611

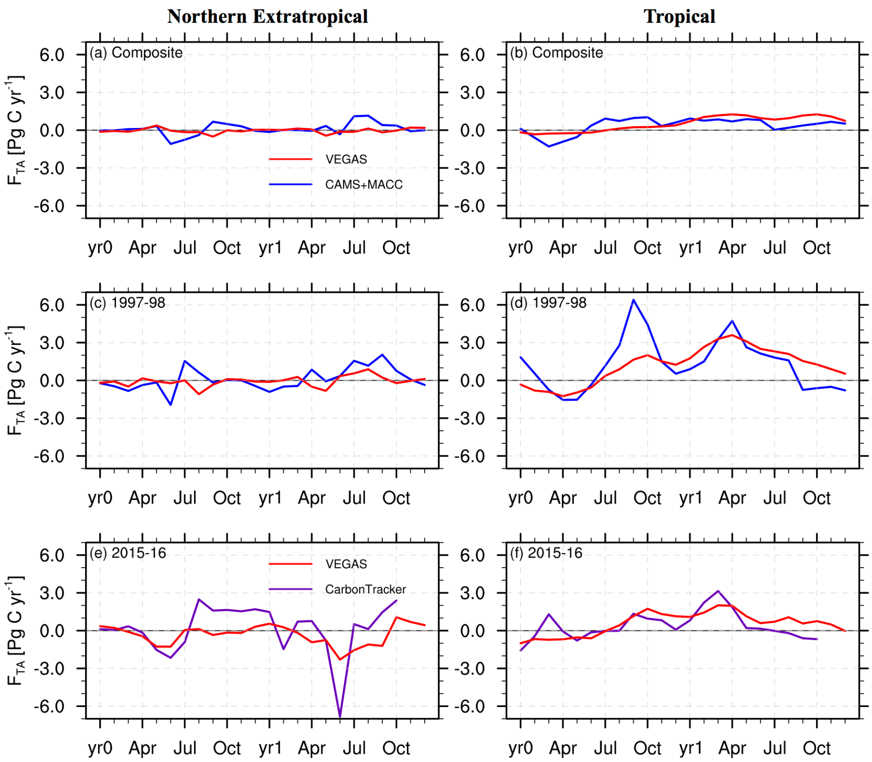

612

613 **Figure 3**. Evolutions of F_{TA} over the extratropical northern hemisphere and tropical
614 regions along with the development of El Niño. (a–b) show the composite results with
615 VEGAS simulation (red solid line) and mean of CAMS and MACC inversions (blue
616 solid line). (c–d) show the F_{TA} anomalies in 1997-98 El Niño. (e–f) demonstrate the
617 FTA anomalies in 2015-16 El Niño with VEGAS (red solid line) and CarbonTracker
618 (purple solid line).

619

Earth Syst. Dynam. Discuss., doi:10.5194/esd-2017-46, 2017
Manuscript under review for journal Earth Syst. Dynam.
Discussion started: 24 May 2017

Earth System Dynamics
Open Access
Discussions

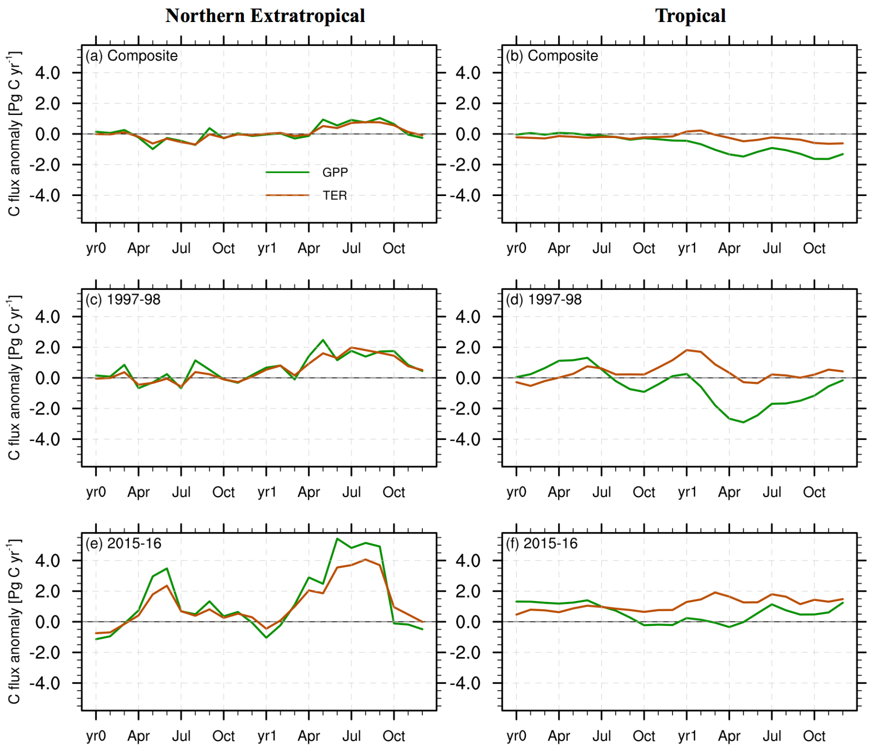

Figure 4. Evolutions of gross primary productivity (GPP, green lines) and terrestrial ecosystem respiration (TER, brown lines) over the extratropical northern hemisphere and tropical regions along with the development of El Niño. (a–b) show the El Niño composite results. (c–d) show the results in 1997-98 El Niño event. And (e–f) demonstrate the results in 2015-16 El Niño event.

Earth Syst. Dynam. Discuss., doi:10.5194/esd-2017-46, 2017
Manuscript under review for journal Earth Syst. Dynam.
Discussion started: 24 May 2017

Earth System Dynamics
Discussions
Open Access

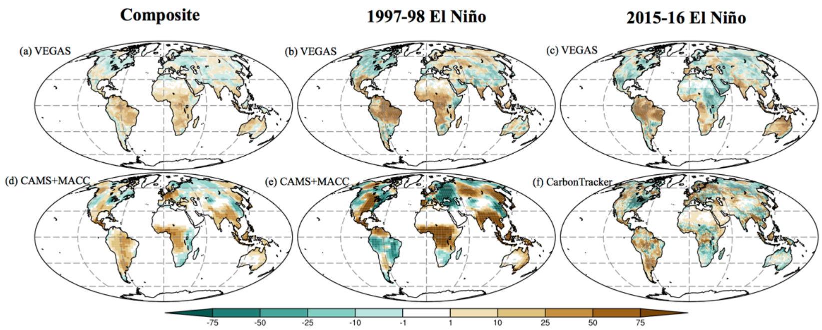

Figure 5. Spatial F_{TA} anomalies calculated from July in El Niño developing year to October in El Niño decaying year (units: Pg C yr^{-1}). (a), (b), and (c) show the results of composite, 1997-98, and 2015-16 El Niño events simulated by VEGAS, respectively. (d) and (e) represent the averaged results of CAMS and MACC in composite and 1997-98 El Niños. (f) shows 2015-16 El Niño F_{TA} anomaly in CarbonTracker.

Earth Syst. Dynam. Discuss., doi:10.5194/esd-2017-46, 2017
Manuscript under review for journal Earth Syst. Dynam.
Discussion started: 24 May 2017

Earth System Dynamics
Discussions

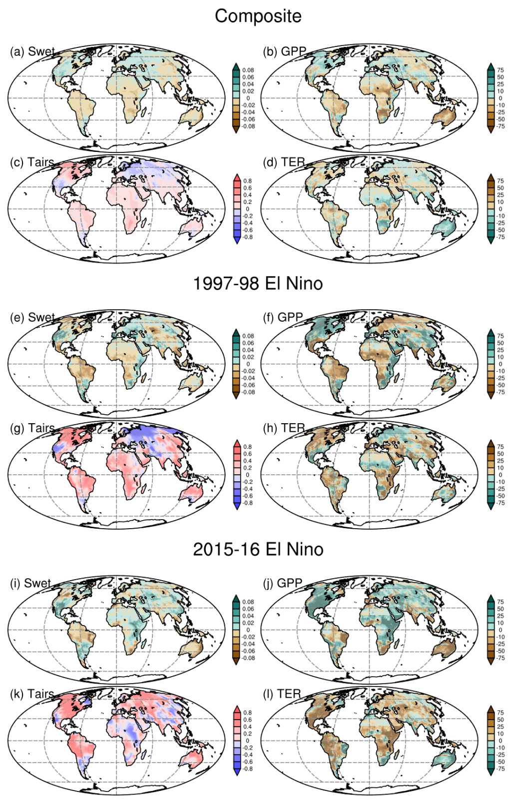

Figure 6. Anomalies in soil wetness, air temperature (units: K), gross primary productivity (GPP, g C m^{-2} yr^{-1}), and terrestrial ecosystem respiration (TER, g C m^{-2} yr^{-1}) from July in El Niño developing year to October in El Niño decaying year in composite, 1997-98, and 2015-16 El Niño episodes, respectively. (a–d) represent the results in composite analyses. (e–h) represent the anomalies during 1997-98 El Niño episode. And (i–l) show the anomalies during 2015-16 El Niño episode.

Earth Syst. Dynam. Discuss., doi:10.5194/esd-2017-46, 2017
Manuscript under review for journal Earth Syst. Dynam.
Discussion started: 24 May 2017

Earth System Dynamics
Discussions

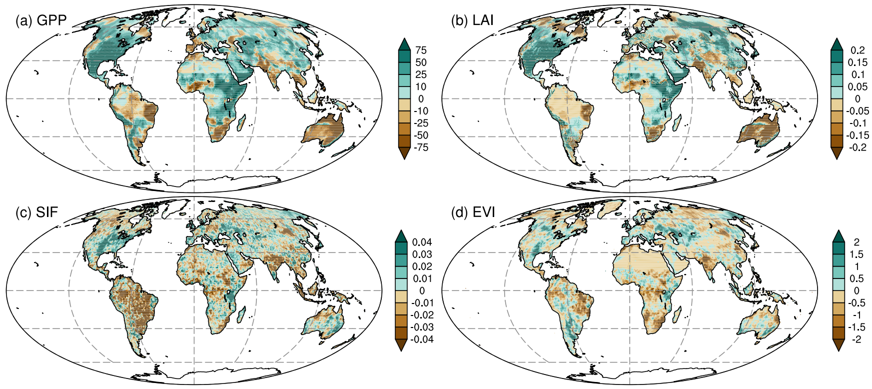

Figure 7. Spatial anomalies in (a) simulated GPP by VEGAS (units: g C m^{-2} yr^{-1}), (b) simulated leaf area index (LAI, units: m^2 m^{-2}), (c) solar-induced chlorophyll fluorescence (SIF, units: mW m^{-2} nm^{-1} sr^{-1}), and (d) MODIS enhanced vegetation index (EVI, $\times 10^{-2}$) from July 2015 to October 2016.

Earth Syst. Dynam. Discuss., doi:10.5194/esd-2017-46, 2017
Manuscript under review for journal Earth Syst. Dynam.
Discussion started: 24 May 2017

Earth System Dynamics
Open Access
Discussions

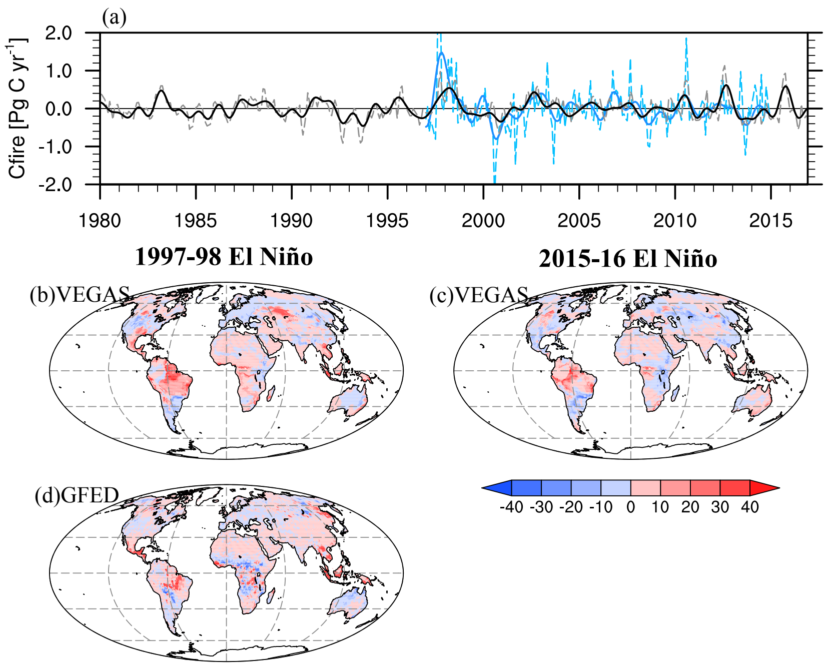

Figure 8. F_{TA} anomalies induced by wildfires. (a) global total anomalies (Pg C yr^{-1}). The dashed gray and solid black lines represent the detrended and smoothed by butterworth filtering anomalies simulated by VEGAS. The dashed and solid blue lines represent the GFED results. (b) spatial F_{TA} anomaly (g C m^{-2} yr^{-1}) in 1997-98 El Niño episode in VEGAS. (c) spatial F_{TA} anomaly in 2015-16 El Niño episode in VEGAS. (d) GFED anomaly in 1997-98 El Niño episode.